Forest Ecosystems 13 (2025) 100322

Contents lists available at ScienceDirect

Forest Ecosystems

journal homepage: www.keaipublishing.com/cn/journals/forest-ecosystems

Nonlinear multilevel seemingly unrelated height-diameter and crown length mixed-effects models for the southern Transylvanian forests, Romania

Albert Ciceu [a,*], Ştefan Leca [b], Ovidiu Badea [b,c], Lauri Mehtätalo [d]

[a] Austrian Research Center for Forests (BFW), Seckendorff-Gudent-Weg 8, 1130, Vienna, Austria
[b] National Institute for Research and Development in Forestry "Marin Drăcea" - INCDS, Blvd. Eroilor, 128, Voluntari, 077190, Ilfov, Romania
[c] Transilvania University, Faculty of Silviculture and Forest Engineering, 1, Ludwig van Beethoven Street, Braşov, 500123, Romania
[d] Luonnonvarakeskus (Luke), Yliopistokatu 6, 80100, Joensuu, Finland

ARTICLE INFO

Keywords:
Multivariate model
Cross-model calibration
Crown allometry
Multilevel model
Mixed stands
Heterogeneous stand structure

ABSTRACT

In this study, we used an extensive sampling network established in central Romania to develop tree height and crown length models. Our analysis included more than 18,000 tree measurements from five different species. Instead of building univariate models for each response variable, we employed a multivariate approach using seemingly unrelated mixed-effects models. These models incorporated variables related to species mixture, tree and stand size, competition, and stand structure. With the inclusion of additional variables in the multivariate seemingly unrelated mixed-effects models, the accuracy of the height prediction models improved by over 10% for all species, whereas the improvement in the crown length models was considerably smaller. Our findings indicate that trees in mixed stands tend to have shorter heights but longer crowns than those in pure stands. We also observed that trees in homogeneous stand structures have shorter crown lengths than those in heterogeneous stands. By employing a multivariate mixed-effects modelling framework, we were able to perform cross-model random-effect predictions, leading to a significant increase in accuracy when both responses were used to calibrate the model. In contrast, the improvement in accuracy was marginal when only height was used for calibration. We demonstrate how multivariate mixed-effects models can be effectively used to develop multi-response allometric models that can be easily calibrated with a limited number of observations while simultaneously achieving better-aligned projections.

1. Introduction

Trees biomass accumulation depends, among other factors, on the amount of photosynthetically active radiation intercepted (Stenberg et al., 1994; Oliveira et al., 2024). The quantity of intercepted photosynthetically active radiation directly correlates with crown architecture, which can be roughly estimated by measuring crown length and width (Zhu et al., 2021). Throughout its life, a tree's crown architecture is shaped by its interactions with surrounding trees and is strongly influenced by its position within the stand's vertical structure (Lintunen and Kaitaniemi, 2010). However, the current crown architecture reflects not only the legacy of past competitive dynamics within the stand but also serves as an indicator of the tree's future growth potential (Mäkelä and Valentine, 2006; Pretzsch, 2021). Therefore crown architecture variables are commonly used to predict tree growth because of their relevance to individual tree biomass accumulation (Weiskittel et al., 2011; Burkhart and Tomé, 2012).

Many of the individual tree growth models include crown characteristics such as height to the crown base (HCB), tree crown length (CL) (e.g., the difference between total tree height (*H*) and HCB), or crown ratio (CR, calculated as the ratio between CL and *H*), in key equations used for predicting tree growth and stand yield. For example, SILVA and MOSES individual tree growth models (Pretzsch et al., 2002; Thurnher et al., 2017) use CR to predict the diameter increment while in PROGNAUS model CR is used as a predictor of tree mortality (Monserud and Sterba, 1999). The SORTIE-ND model utilizes CL, whereas the ORGANON and Forest Vegetation Simulator Northeastern Variant (FVS-NE) models predict HCB for use in their sub-models (Hann et al., 2011; Sattler and LeMay 2011; Rijal et al., 2012).

Like those described above, crown characteristic models rely on *H*,

* Corresponding author.
E-mail addresses: albert.ciceu@bfw.gv.at (A. Ciceu), stefan.leca@icas.ro (Ş. Leca), obadea@icas.ro (O. Badea), lauri.mehtatalo@luke.fi (L. Mehtätalo).
Peer review under the responsibility of Editorial Office of Forest Ecosystems.

https://doi.org/10.1016/j.fecs.2025.100322
Received 24 September 2024; Received in revised form 12 February 2025; Accepted 5 March 2025

among other variables, as a crucial predictor. Tree H is closely associated with crown characteristics because it governs the degree of natural pruning experienced by the trees. Typically, taller trees have longer crowns due to their increased access to light, while suppressed trees tend to have smaller crowns due to the shade cast by the taller trees. When tree H is not measured directly, it is predicted by another univariate model using variables such as diameter at breast height (DBH) and other stand characteristics (Calama and Montero, 2004; Trincado et al., 2007; Yang et al., 2022). This results in a cascade of predictions within the architecture of an individual tree growth model (Eq. 1), leading to strong cross-equation correlations that can impact the model's behaviour (Hasenauer et al., 1998).

$$\begin{aligned} H &= f_1(\mathrm{DBH}) + \epsilon_1 \\ \mathrm{CL} &= f_2(\mathrm{DBH}, \widehat{H}) + \epsilon_2 \\ &\vdots \\ Y &= f_n(\mathrm{DBH}, \widehat{H}, \widehat{\mathrm{CL}}, \ldots, \widehat{X}_{n-1}) + \epsilon_n \end{aligned} \tag{1}$$

where Y is the n-th variable predicted in the individual growth model, $\widehat{X}$ represents the $n-1$ previously predicted variable, and ϵ is the error term. The other variables have been explained earlier in the text.

Instead of developing n separate univariate models for each variable in an individual growth model and using the predicted values as additional predictors, one could leverage the relationships between the variables by employing a multivariate model. This approach allows for the estimation of cross-model correlation of residual errors. Moreover, if the data are organized hierarchically, the correlation between the random-effects parameters of the models can be estimated, enabling cross-model calibration when new observations become available.

A model of this nature could be developed using a multivariate seemingly unrelated mixed-effects framework. The application of seemingly unrelated regression (SUR), as introduced by Zellner (1962), has been explored in forest science by Hasenauer et al. (1998), who simultaneously fitted a system of three equations: H, basal area, and CR. An extension of SUR to hierarchical data was demonstrated by Lappi (1991), Eerikäinen (2009), and Bronisz and Mehtätalo (2020b), who developed multivariate models involving H and tree volume, H and CR, as well as H and tree biomass components, respectively. These approaches facilitated the cross-calibration of tree volume, CR, and biomass components when new H observations were available. It is important to highlight that the models used in the aforementioned studies were linear. An application of a multivariate nonlinear mixed-effects modelling framework was presented by Hall and Clutter (2004), who developed a trivariate three-level model that simultaneously fitted three stand characteristics, dominant height, basal area and the number of trees per hectare. This approach provided more realistic predictions of current and future plot-level timber characteristics while preserving the inherently nonlinear relationships between the response and predictor variables.

In line with this approach, our study aims to achieve two key objectives. First, using a nonlinear multilevel multivariate mixed-effects modelling framework, we seek to develop H and CL models tailored to the Transylvania region for five economically significant species. Second, using the same modelling framework we aim to estimate the cross-model correlation of residual errors and random effects, enabling us to not only calibrate the full multivariate model but also perform cross-calibration between the models when new observations are available.

2. Methods

2.1. Location

In 2019, a collaboration was established between the Romanian National Institute of Research and Development in Forestry "Marin Drăcea" - INCDS and the Local Public Forest Administration Kronstadt R.A. (LPFAK). The primary objective of this partnership was to conduct a comprehensive inventory of the 14,262.7 ha of forest administered by LPFAK.

The focus was on monitoring the state of forest ecosystems and capitalizing on the recreational, cultural, and historical ecosystem services provided by urban and peri-urban forests. These forests are situated in the surroundings of Braşov, a city historically known by its German name, Kronstadt (meaning *"City of the Crown"*). The city is located in central Romania in the southeastern part of the Transylvania region (Fig. 1).

2.2. Forest inventory

The forests administered by LPFAK are divided into six production units (PU) for administrative purposes, in accordance with Romanian forest management planning regulations. For each of these PU, a systematic network of cluster units (CU) was designed to estimate the standing volume with an accuracy of 10% at a 95% confidence interval. A cluster sampling network was preferred due to its increased logistical efficiency and the ability to yield a relatively large amount of data, making it a common design choice, especially for large-scale forest inventories (Badea and Patrascoiu, 1999; Badea, 2008; Tomppo et al., 2010; Leca et al., 2023). The number and spacing of CU were determined based on the variability of the stand volume as estimated in the management plans, the target accuracy, and the desired confidence interval (Cochran, 1963; Giurgiu, 1968). The Romanian forest management system is centralized, meaning that a uniform set of rules, practices, and guidelines is applied to all forests across the country, regardless of ownership. Forest management plans promote highly diverse forest stands by implementing regeneration schemes that incorporate multiple species. Rotation periods for most species exceed 100 years, reaching up to 160 years for highly productive stands. Assisted natural regeneration is the main method for reestablishing forests after harvest, leading to structurally diverse stands due to the extended regeneration periods ranging from 20 to 30 to as long as 60 years.

Due to the variation in altitude, species compositions, and stand age distributions of each PU, the standing volume varied accordingly, influencing the number of CU and the distance between them (Table 1).

Each CU is composed of two circular subplots (SP). The centre of each SP is located 30 m from the CU central location (Ciceu et al., 2021). If one SP fell outside the forested area, only one SP was installed. The size of the SP varies: for trees with a maximum diameter of less than 28 cm, the SP is 200 m^2 ($r = 7.98$ m); for trees with a larger maximum diameter, the SP is 500 m^2 ($r = 12.62$ m).

2.3. Data

In each SP, all trees with DBH greater than 8 cm were measured, resulting in a total of 23,250 trees sampled belonging to 35 tree species. Of these, 22,637 trees were measured for H and 20,045 trees were measured for both H and HCB. In the sampling protocol, HCB was defined as the vertical distance along the main stem of a tree from its base to the lowest point where continuous live branches form the full crown. Tree DBH measurements were taken using a tape band to the nearest mm, while H measurements were conducted using the VERTEX IV hypsometer. The main five species measured were European beech (*Fagus sylvatica* L.), representing 48% of the measured trees, followed by Norway spruce (*Picea abies* (L.) Karst.) and silver fir (*Abies alba* Mill.) at 27.1% and 10%, respectively. Sycamore maple (*Acer pseudoplatanus* L.) and European hornbeam (*Carpinus betulus* L.) accounted for 5.4% and 5%. Except for sessile oak (*Quercus petraea* (Matt.) Liebl.), all other species represented less than 1% of the measurements. For our analysis, we excluded dead trees, trees with a broken or dead top, double-stemmed trees, and leaning trees, as these factors strongly bias H measurements. We focused exclusively on European beech (BE), Norway spruce (SPR), silver fir (FIR), sycamore maple (SYM), and European hornbeam (EH) as this selection provided a substantial sample of H-DBH and CL-DBH measurement pairs (Table 2).

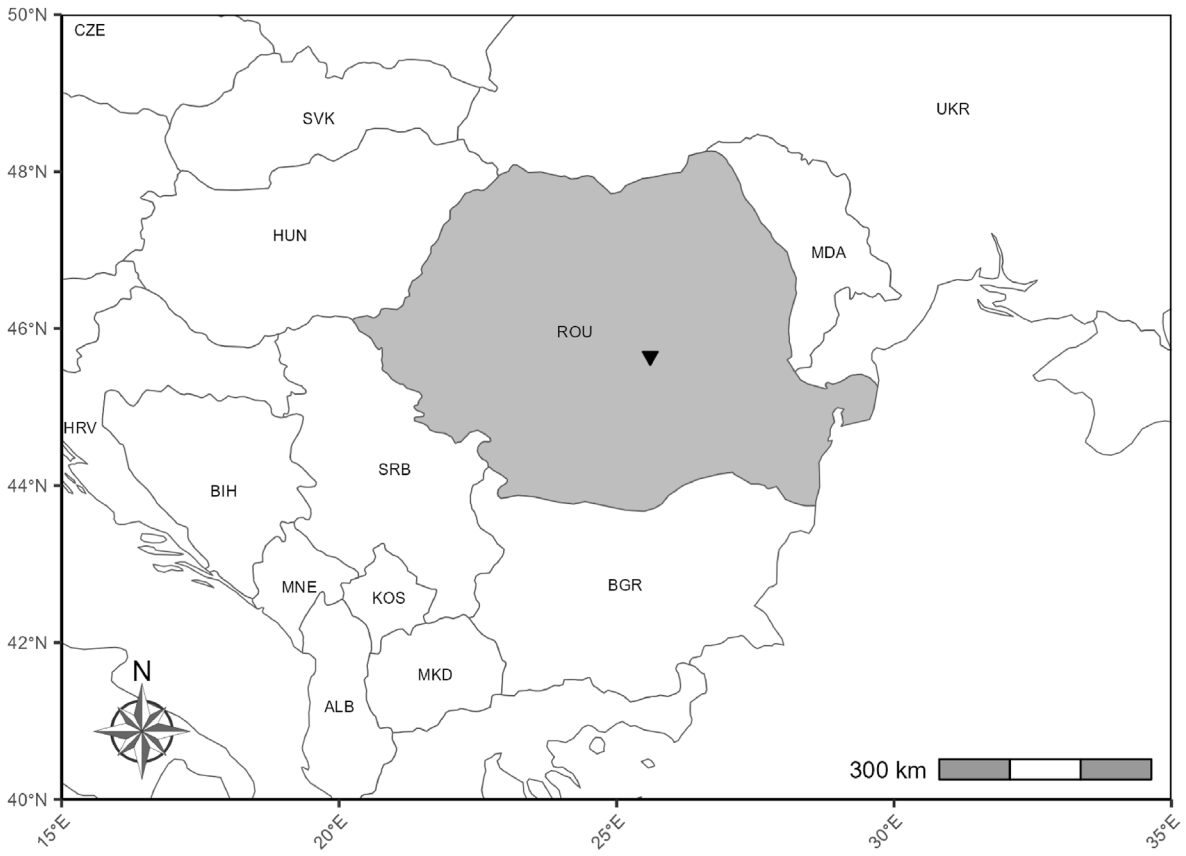

Fig. 1. Study area. The grey-shaded region represents the territory of Romania, with the marker indicating the location of Braşov, where the six inventory networks were established. A detailed view of the inventory networks is available in the KML file attached to the Supplementary Material of this article.

Table 1
Planned and established CU and SP, along with the distance between CU in each PU.

PU	Planned CU	Distance between CU (m)	Established	
			CU	SP
I	90	400	77	142
II	73	750	72	144
III	79	700	72	139
IV	69	650	65	125
V	62	400	52	101
VI	75	350	69	132

2.4. Simple multilevel H-DBH and CL models

In a preliminary analysis, not included in this paper, we found a stronger cross-model correlation of residuals between the *H*-DBH and CL-DBH models compared to HCB or CR models. Moreover, we observed a more favourable distribution of residuals in the fitted CL models due to the absence of an imposed asymptote, unlike the CR models. For this reason, we chose to predict CL (the difference between *H* and HCB) simultaneously with *H*. For this purpose, we chose to test four widely used two-parameter models known as: Curtis (1967) - Eq. 2, Näslund (1936), Schumacher (1939) - Eq. 4, and Wykoff et al. (1982) - Eq. 5. The same equations were tested for predicting both the *H* and CL and their formulations are

$$y = \mathrm{bh} + a\left(\frac{\mathrm{DBH}}{1+\mathrm{DBH}}\right)^{b} \tag{2}$$

$$y = \mathrm{bh} + \frac{\mathrm{DBH}^2}{[a+\exp(b\times \mathrm{DBH})]^2} \tag{3}$$

$$y = \mathrm{bh} + a\exp\left(\frac{-b}{\mathrm{DBH}}\right) \tag{4}$$

$$y = \mathrm{bh} + \exp\left(a + \frac{b}{\mathrm{DBH}+1}\right) \tag{5}$$

where *a* and *b* are the function's parameters, bh is the height at which the tree diameter measurements were taken (1.3 m when predicting *H* and

Table 2
Summary of DBH, *H*, and HCB measurements for the main five species in the study area.

Species	*N*	DBH (cm)				*H* (m)				HCB (m)			
		min	max	mean	sd	min	max	mean	sd	min	max	mean	sd
BE	9430	8.0	115.7	23.8	14.8	3.1	48.1	19.9	7.8	0.1	29.8	10.6	4.9
SPR	4471	8.1	98.4	32.4	15.3	3.0	48.1	24.3	8.9	0.2	34.0	13.1	6.1
FIR	1818	8.0	106.8	30.7	20.6	3.2	52.0	20.9	11.4	0.2	35.1	11.4	7.7
SYM	1000	8.1	74.4	20.8	11.1	4.8	40.0	18.8	5.9	1.5	27.5	11.0	4.1
EH	949	8.0	68.8	16.6	7.5	4.1	31.2	16.9	4.8	0.1	20.6	8.3	3.5

0 when predicting CL), y is the response variable (H or CL in our case). The 1.3 m constant is frequently applied to H-DBH models to ensure a consistent representation of small trees, forcing the curve to pass and $H = 1.3$ point when DBH = 0. However, this constraint also results in a zero slope at that point, which is not a realistic assumption and imposes limitations on the shape of the H curve. To improve the model while maintaining logical behaviour, Siipilehto et al. (2023) proposed two additional parameters that allow greater accuracy of the H-DBH curve especially for small DBH. In our case, we did not specifically address this issue, as our dataset included trees with DBH values of at least 8 cm and H exceeding 1.3 m.

The models were fitted using nonlinear mixed-effects using the *nlme* function of the 'nlme' package (R Core Team, 2022). Both parameters were considered random with two levels of hierarchy: CU and SP for each of the five species.

A nonlinear mixed-effect model with two levels of nesting can be written as Pinheiro and Bates (2000).

$$\begin{aligned} \boldsymbol{y}_{ijk} &= \boldsymbol{f}\left(\boldsymbol{\phi}_{ijk}, \boldsymbol{v}_{ijk}\right) + \boldsymbol{\epsilon}_{ijk}, \\ & i = 1, \ldots, M,\ j = 1, \ldots, M_i,\ k = 1, \ldots, n_{ij}, \end{aligned} \tag{6}$$

where $\boldsymbol{y}_{ijk}$ denotes the response variable, $\boldsymbol{f}$ is a response function that is nonlinear in at least one component of $\boldsymbol{\phi}_{ij}$, and $\boldsymbol{v}_{ijk}$ and $\boldsymbol{\phi}_{ij}$ are covariate and group-specific parameter vectors, respectively. M represents the number of first-level groups (in our case, CU), M_i is the number of second-level groups within the i-th first-level group (in our case, SP), n_{ij} denotes the number of observations in the j-th second-level group of the i-th first-level group, and $\boldsymbol{\epsilon}_{ijk}$ is a normally distributed within-group error term.

To address heteroscedasticity in the residuals ($\boldsymbol{\epsilon}_{ijk}$), var($\boldsymbol{\epsilon}_{ijk}$) was modelled as a function of DBH while $\boldsymbol{\sigma}^2$ and $\boldsymbol{\delta}$ were used as the scale and shape parameters of a power-type variance function $\left(\mathrm{var}(\boldsymbol{\epsilon}_{ijk}) = \boldsymbol{\sigma}^2 \mathrm{DBH}_{ijk}^{2\boldsymbol{\delta}}\right)$ where k is a tree from SPj belonging to the i-th CU.

The parameter vector $\boldsymbol{\phi}_{ij}$ can be expressed as:

$$\begin{aligned} \boldsymbol{\phi}_{ijk} &= \boldsymbol{A}_{ijk}\boldsymbol{\beta} + \boldsymbol{B}_{i,jk}\boldsymbol{b}_i + \boldsymbol{B}_{ijk}\boldsymbol{b}_{ij}, \\ \boldsymbol{b}_i &\sim \mathcal{N}(0, \boldsymbol{D}_1), \\ \boldsymbol{b}_{ij} &\sim \mathcal{N}(0, \boldsymbol{D}_2) \end{aligned} \tag{7}$$

where $\boldsymbol{\beta}$ is a vector of fixed-effects, $\boldsymbol{A}_{ijk}$ is the fixed-effects design matrix, $\boldsymbol{B}_{i,jk}$ and $\boldsymbol{B}_{ijk}$ are the random-effects design matrices, whose sizes depend on the group; $\boldsymbol{b}_i$ are first-level random-effects with variance-covariance matrix $\boldsymbol{D}_1$, $\boldsymbol{b}_{ij}$ are second-level random-effects with variance-covariance matrix $\boldsymbol{D}_2$. Both random-effects vectors are independently distributed and assumed to be independent of each other.

Two models were obtained for each species, one for H and one for CL. The best-performing model was determined based on root mean squared error (RMSE) and mean error (ME). RMSE and ME were computed for both fixed-effects predictions and fixed and random-effects predictions. A relative ranking score (Eq. 8) was calculated based on the goodness-of-fit obtained from each evaluation statistic and prediction. The model with the lowest combined rank across all evaluation statistics was further developed and considered the best-performing model.

$$R_m = 1 + \frac{(n-1)(S_m - S_{\min})}{S_{\max} - S_{\min}} \tag{8}$$

where R_m is the relative rank with m taking values between 1 and 4, corresponding to the four functions tested, S_m represents the RMSE or ME values obtained from fixed or fixed and random-effect predictions, and $S_{\min}$ and $S_{\max}$ denote the minimum and maximum values of S_m.

2.5. Additional predictors

Additional predictors were tested to improve the applicability and accuracy of the models. For the H-DBH model, the primary predictors considered were stand-level predictors, including quadratic mean diameter (Dg), number of trees per hectare (N), total basal area per hectare (G) and dominant diameter (Ddom) calculated as the thickest 100 trees per hectare.

For the CL model, additional predictors were computed to model competition effects at the tree level. We tested three distance-independent competition indexes: the relative position index (RD - Eq. 9), the basal area of larger trees (BAL - Eq. 10), and a combined competition index (BALMOD - Eq. 11) that integrates BAL with a modified version of the relative spacing index (RS - Eq. 12). To capture the complex stand structure of Romanian forests, we also tested the Gini index (Eq. 13) in our models. We calculated the Gini index based on the DBH values of each SP and since is typically calculated from a complete inventory, we included it exclusively in the CL model. The formulations of the additional computed predictors are

$$\mathrm{RD}_{ijk} = \frac{\mathrm{DBH}_{ijk}}{\mathrm{Dg}_{ij}} \tag{9}$$

$$\mathrm{BAL}_{ijk} = G_{ij} - p_{ijk} \tag{10}$$

$$\mathrm{BALMOD}_{ijk} = \frac{1 - p_{ijk}}{\mathrm{RS}_{ij}} \tag{11}$$

$$\mathrm{RS}_{ij} = \frac{\sqrt{10000/N_{ij}}}{\mathrm{Dg}_{ij}} \tag{12}$$

$$\mathrm{Gini}_{ij} = \frac{\sum_{k=1}^{n_{ij}} (2k - n_{ij} - 1)\mathrm{DBH}_{ijk}}{\sum_{k=1}^{n_{ij}} \mathrm{DBH}_{ijk} n_{ij}} \tag{13}$$

where p_{ijk} represents the basal area percentile of the k-th tree in the j-th SP within the i-th CU, and n_{ij} denotes the total number of observations in that sampling plot. Detailed explanations of other notations are provided earlier in the text.

2.6. Extended univariate models

Due to the significant computational time required for species with extensive measurement datasets, fitting, testing, and comparing multivariate models proved to be challenging. Therefore, we decided to select predictors based on the fit of univariate models. We tested various combinations and transformations of the additional predictors. The models were then compared based on the RMSE, ME, and estimated information loss, as determined by likelihood functions in the Akaike Information Criterion (AIC) and conditional F-tests. We employed a nonlinear mixed-effects framework to fit the extended models, using the same statistical package as for the simple models. The same two levels of grouping were specified: SP and CU. In all models, intercept parameters were treated as random, and heteroscedasticity was accounted for.

Given that most SPs comprised multiple species, various variables were computed to model species composition. A dummy variable approach was used to code mixed SPs as 1 and others as 0, or to identify dominant species as 1 and 0 otherwise. Species share per ha $\left(\frac{G_{\text{species}}}{G}\right)$ and the basal area of the species per ha (G_{species}) were tested as well as additional predictors for both models.

2.7. Nonlinear multilevel seemingly unrelated mixed-effects models (NSURME)

Seemingly unrelated regression is commonly used to model the interactions among individual statistical relationships. When the data has a hierarchical structure, it can be extended to mixed-effects models, allowing for the estimation of random-effects correlation between these individual relationships. A detailed display of multivariate linear mixed-effects model formulation, fitting procedure and calibration is provided

by Mehtatalo and Lappi (2020). The adaptation to nonlinear models is discussed in the following sections.

Assuming we have a system of L individual nonlinear mixed-effects models (Eq. 6), a multivariate seemingly unrelated mixed-effects model system with two levels of grouping i and j, and pooled response of ij grouping in the $\boldsymbol{y}_{ij}$ vector, can be written as follows:

$$\begin{aligned} \boldsymbol{y}_{ij}^{(1)} &= \boldsymbol{f}\left(\boldsymbol{\phi}_{ij}^{(1)}, \boldsymbol{v}_{ij}^{(1)}\right) + \boldsymbol{\epsilon}_{ij}^{(1)} \\ \boldsymbol{y}_{ij}^{(2)} &= \boldsymbol{f}\left(\boldsymbol{\phi}_{ij}^{(2)}, \boldsymbol{v}_{ij}^{(2)}\right) + \boldsymbol{\epsilon}_{ij}^{(2)} \\ &\vdots \\ \boldsymbol{y}_{ij}^{(L)} &= \boldsymbol{f}\left(\boldsymbol{\phi}_{ij}^{(L)}, \boldsymbol{v}_{ij}^{(L)}\right) + \boldsymbol{\epsilon}_{ij}^{(L)} \end{aligned} \tag{14}$$

To fit a nonlinear multilevel seemingly unrelated mixed-effects model, we formulated our model as a single-response model $\left(\boldsymbol{y}_{ij} = \left(\boldsymbol{y}_{ij}^{(1)'}, \boldsymbol{y}_{ij}^{(2)'}, \ldots, \boldsymbol{y}_{ij}^{(L)'}\right)'\right)$. We created a single data matrix, stacking the H and CL response variables and the corresponding predictors for each sampling unit. The univariate matrix formulation for a multivariate model can be written as

$$\boldsymbol{y}_{ij} = \begin{bmatrix} \boldsymbol{y}_{ij}^{(1)} \\ \boldsymbol{y}_{ij}^{(2)} \\ \vdots \\ \boldsymbol{y}_{i}^{(L)} \end{bmatrix}, \boldsymbol{\phi}_{ij} = \begin{bmatrix} \boldsymbol{\phi}_{ij}^{(1)} \\ \boldsymbol{\phi}_{ij}^{(2)} \\ \vdots \\ \boldsymbol{\phi}_{ij}^{(L)} \end{bmatrix}, \boldsymbol{v}_{ij} = \begin{bmatrix} \boldsymbol{v}_{ij}^{(1)} & 0 & \cdots & 0 \\ 0 & \boldsymbol{v}_{ij}^{(2)} & \cdots & 0 \\ \vdots & \vdots & \ddots & \vdots \\ 0 & 0 & \cdots & \boldsymbol{v}_{ij}^{(L)} \end{bmatrix}, \boldsymbol{\epsilon}_{ij} = \begin{bmatrix} \boldsymbol{\epsilon}_{ij}^{(1)} \\ \boldsymbol{\epsilon}_{ij}^{(2)} \\ \vdots \\ \boldsymbol{\epsilon}_{ij}^{(L)} \end{bmatrix}$$

where $\boldsymbol{\phi}_{ij}$ was modelled as in Eq. 7 with the appropriate fixed-effects ($\boldsymbol{A}_{ij}$) and random-effects design matrices ($\boldsymbol{B}_{i,j}$, $\boldsymbol{B}_{ij}$) and their corresponding random-effects vectors $\boldsymbol{b}_i$ and $\boldsymbol{b}_{ij}$. We specified response-specific random-effects and different variances for each response. Similar to the simple models the multilevel nonlinear seemingly unrelated mixed-effect models were fitted using nonlinear mixed-effects using the *nlme* function of the 'nlme' package (R Core Team, 2022). An R script detailing the model fitting procedure and data structure preparation is provided in the Supplementary Material.

2.8. Calibrating the model when new observations are available

One of the main advantages of mixed-effects models is that the random-effects can be predicted for a new plot if observations of the response variable are available, otherwise, just the fixed-effects can be used (Trincado et al., 2007; Bronisz and Mehtätalo, 2020a; Ciceu et al., 2020).

In our study, we considered two scenarios to predict random-effects which can occur in practice. The first scenario occurs when both response variables' observations are available in an inventory plot. For such a case the random-effects prediction is based on the linear approximation of $\boldsymbol{y}_{ij} = \boldsymbol{X}_{ij}\boldsymbol{\beta} + \boldsymbol{Z}_{i,j}\boldsymbol{b}_i + \boldsymbol{Z}_{ij}\boldsymbol{b}_{ij} + \boldsymbol{\epsilon}_{ij}$, where $\boldsymbol{X}_{ij}$, $\boldsymbol{Z}_{i,j}$ and $\boldsymbol{Z}_{ij}$ includes the partial derivatives of the nonlinear function with respect to parameters $\boldsymbol{\beta}$, $\boldsymbol{b}_i$ and $\boldsymbol{b}_{ij}$, respectively. For two levels of grouping if we pool the two levels of random-effects we have

$$\boldsymbol{b}_i = \begin{pmatrix} \boldsymbol{b}_i \\ \boldsymbol{b}_{ij} \end{pmatrix}, \boldsymbol{Z}_i = \begin{pmatrix} \boldsymbol{Z}_{i,j} & \boldsymbol{Z}_{ij} \end{pmatrix}.$$

For this situation where both of the response variables are available, random-effects can be predicted using the best linear unbiased predictors (BLUP) (Mehtatalo and Lappi, 2020):

$$\widehat{\boldsymbol{b}_i} = \widehat{\boldsymbol{D}}\boldsymbol{Z}_i^T\left(\widehat{\boldsymbol{R}}_i + \boldsymbol{Z}_i\widehat{\boldsymbol{D}}\boldsymbol{Z}_i^T\right)^{-1}\left[\boldsymbol{y}_i - \boldsymbol{f}(\boldsymbol{v}_i, \widehat{\boldsymbol{\beta}_i}, \widehat{\boldsymbol{b}_i}) + \boldsymbol{Z}_i\widehat{\boldsymbol{b}_i}\right] \tag{15}$$

where $\widehat{\boldsymbol{b}_i}$ is a vector that aggregates all random-effects from the L individual nonlinear mixed effects models and all levels of grouping. $\widehat{\boldsymbol{D}}$ is the variance-covariance matrix of these random-effects, including cross-model variance-covariance estimates. The upper first block consists of the variance at the first level of grouping ($\widehat{\boldsymbol{D}_i}$). The subsequent blocks contain the variance matrices for random-effects at the lower grouping levels ($\widehat{\boldsymbol{D}_{ij}}$). $\widehat{\boldsymbol{R}_i}$ represents the cross-model variance-covariance of residual errors, capturing the correlation between the residual errors of the two individual models. The diagonal matrix includes $\boldsymbol{\sigma}^2$ estimates based on the variance functions of the two individual nonlinear mixed effects models. The calibration is implemented using a straightforward nonlinear mixed effects calibration.

The second scenario considered was when only H measurements were available in the inventory. In this case, if all fixed-effects covariates are available for both individual mixed-effects models, cross-model random-effects prediction is possible and recommended. In this case, the random-effects are predicted based on the best linear predictor (Mehtatalo and Lappi, 2020)

$$\grave{\widehat{\boldsymbol{b}_i}} = \grave{\widehat{\boldsymbol{C}}}\grave{\boldsymbol{Z}_i}^T\left(\grave{\widehat{\boldsymbol{R}}}_i + \grave{\boldsymbol{Z}_i}^T\grave{\widehat{\boldsymbol{D}}}\grave{\boldsymbol{Z}_i}^T\right)^{-1}\left[\grave{\boldsymbol{y}_i} - \boldsymbol{f}(\grave{\boldsymbol{v}_i}, \grave{\widehat{\boldsymbol{\beta}}_i}, \grave{\widehat{\boldsymbol{b}_i}}) + \grave{\boldsymbol{Z}_i}\grave{\widehat{\boldsymbol{b}_i}}\right] \tag{16}$$

where vector $\grave{\boldsymbol{y}_i}$ contains only the observed responses, along with the corresponding predictors $\grave{\boldsymbol{v}_i}$ and fixed-effects parameters $\grave{\widehat{\boldsymbol{\beta}}_i}$. The matrices $\grave{\boldsymbol{Z}_i}$, $\grave{\widehat{\boldsymbol{R}}_i}$, and $\grave{\widehat{\boldsymbol{D}}}$ are constructed by removing the rows and columns corresponding to the unobserved responses, in our case the CL, from the corresponding matrices ($\widehat{\boldsymbol{Z}_i}$, $\widehat{\boldsymbol{R}_i}$ and $\widehat{\boldsymbol{D}}$).

A detailed numerical example, including definitions of all terms and a step-by-step guide for predicting the random-effects under the two scenarios, is provided in Supplementary Material Appendix A. This example is accompanied by the R script implementation, which is also available in the Supplementary Material.

Several studies have highlighted the importance of sampling strategies in enhancing accuracy when predicting random-effects for new plots (Bronisz and Mehtätalo, 2020a; Patrício et al., 2022; Ciceu et al., 2023). Our study used the same plots for model fitting to evaluate various sampling strategies. The number of plots used for calibration varied by species due to differences in species abundance across the plots. For BE and SPR, only plots with at least 10 trees of the same species were chosen, while for FIR, plots with at least 8 were selected. For SYM and EH, plots containing at least 6 trees were used.

In the first scenario, where observations for both response variables were available, the CU observations were randomly divided into calibration and validation datasets. In the second scenario, where only H observations were available, a cross-model random-effects calibration was performed. In this case, the calibration dataset was used to predict the random-effects, while the validation dataset for CL included all trees in the CU, including those trees with H measurements that have been used for calibration. For calibration, 8 trees were used for BE and SPR, 6 trees for FIR, and 4 trees for SYM and EH. In the first scenario, the remaining trees were allocated to the validation dataset. This process was repeated ten times.

During each iteration, we evaluated three distinct sampling strategies with varying numbers of sampled trees: 2, 4, 6, and 8 for BE and SPR; 2, 4, and 6 for FIR; and 2 and 4 for SYM and EH. The first strategy involved randomly selecting trees from the calibration dataset. The second strategy focused on sampling trees from the extremes of the diameter distribution, while the third targeted trees near Dg of the SP. The effectiveness of each calibration strategy was assessed by averaging the RMSE statistic across the ten iterations for each sampling strategy and number of sampled trees.

3. Results

3.1. Simple H-DBH and CL model performance

All two-parameter models demonstrated similar performance, with only minor differences (Supplementary Material Table B1). For the H model prediction, the RMSE based on fixed and random-effects

parameters varied between 1.7 m for SYM and 2.6 m for BE, while for the CL model, the RMSE ranged from 1.5 m for SYM to 2.5 m for EH. Notably, except for SYM, the RMSE based on fixed and random-effects predictions was lower for the *H* model than for the CL model, indicating that the random-effects explain a higher percentage of the variation in the *H* model.

However, a different behaviour is observed when comparing the RMSE of the *H* and CL models based on the fixed-effects parameters only. In this case, for all species and models tested, the RMSE of the CL model is lower than that of the *H* model. This suggests that the variation in CL is lower than the variation in *H* and that DBH alone explains a large percentage of the variation in the CL model.

When investigating ME for the *H* model, ME based on fixed and random-effects parameters varied between −2 and −33 cm. In contrast, the ME based solely on the fixed-effects parameters varied between 8 and 1.06 m. For the CL model, the ME based on fixed and random-effects ranged from −36 to 6 cm, whereas the ME based only on the fixed-effects parameters ranged from −24 to 58 cm.

The relative rank sum showed that the Curtis model consistently ranked first for all five species when predicting *H*. When predicting CL, the Näslund model performed better, consistently ranking on top for four out of five species. Therefore, we decided to move forward with the two models and used the Curtis model for *H* prediction and the Näslund model for CL prediction for all species.

3.2. Nonlinear multilevel seemingly unrelated mixed-effects model formulation

We wrote the two functions as an univariate model using a dummy variable approach (Eq. 17).

$$y_{ijk} = S\left[1.3 + \left(\beta_1^{(1)} + b_i^{(11)} + b_{ij}^{(12)}\right)\left(\frac{\mathrm{DBH}_{ijk}}{1+\mathrm{DBH}_{ijk}}\right)^{\left(\beta_2^{(1)}+b_i^{(13)}+b_{ij}^{(14)}\right)} + e_{ijk}^{(1)}\right] + (1-S)\left[\frac{\mathrm{DBH}_{ijk}}{\left(\beta_3^{(2)} + b_i^{(21)} + b_{ij}^{(22)}\right) + \exp\left(\beta_4^{(2)} + b_i^{(23)} + b_{ij}^{(24)}\right)\mathrm{DBH}_{ijk}}\right]^2 + e_{ijk}^{(2)} \quad (17)$$

where y_{ijk} represents either *H* or CL of tree *k* from SP*j* within CU *i*. The variable *S* is a dummy variable that equals 1 if the response vector y_{ijk} is *H* and 0 if it is CL. Parameters $\beta_1^{(1)}, \ldots, \beta_4^{(2)}$ are the fixed-effects parameters corresponding to the two responses.

3.3. Generalized H-DBH and CL seemingly unrelated mixed-effects models

Each parameter in Eq. 17 was modelled as a linear function of additional predictors, with the intercept included as a random-effect for both SP and CU. However, convergence was not achieved for the SYM and EH species when both intercepts were set as random-effects in the CL model. As a result, only the intercept associated with $\beta_3^{(2)}$ was used. A strong cross-model correlation of residual errors and random-effects was identified for all species varying between 0.462 for SPR to 0.677 for EH (Supplementary Material Table C11). For the *H* model, the natural logarithm transformation of Dg emerged as the primary additional predictor across most species (Table 3. The species mixture was modelled by introducing G_{species} or $\frac{G_{\text{species}}}{G}$, into the function. Most parameters were highly significant ($p < 0.0001$), except the parameter associated with ln(Dg) for SYM species in the *H* model, which had the lowest significance level ($p < 0.1$). However, it was retained in the model due to its biological relevance and because removing it increased the ME of the fixed-effects predictions.

Including additional predictors significantly enhanced the performance of the NSURME model, particularly in predictions based solely on the fixed part. When compared to the simple *H*-DBH univariate model, incorporating these predictors in the NSURME *H* response resulted in a substantial reduction in the RMSE: 13.4% for BE, 12.3% for SPR, 10.6% for FIR, 13.5% for SYM, and 10.7% for EH.

Furthermore, the additional variables had an even more pronounced effect on the ME statistic, resulting in considerable improvements: 95.6% for BE, 92% for SPR, 66.7% for FIR, 81.5% for SYM, and 85.5% for EH.

In contrast, for the CL component of the NSURME model, incorporating additional variables did not enhance RMSE accuracy to the same extent as the *H* component (Table 4). The improvements in RMSE were more modest: 4.6% for BE, 1.3% for SPR, 3.5% for FIR, 3.1% for SYM, and 3% for EH.

However, for the ME statistic, the additional predictors had a similar impact as for the *H* response: 84.3% for BE, 49% for SPR, 51.4% for FIR, 93.7% for SYM, and 98.1% for EH.

Table 3
Fixed parameters corresponding to the *H* model for the main five species in the study area.

Species	Fixed Param.	Term	Estimate	Std. Error
BE	$\beta_1^{(1)} \sim$	Intercept	−40.142	3.119
BE		ln(Dg)	23.360	1.152
BE		$\ln(G_{\text{species}})$	1.509	0.200
BE		Ddom	−0.189	0.029
BE	$\beta_2^{(1)} \sim$	Intercept	−3.005	2.528
BE		ln(Dg)	5.791	0.641
BE		$\sqrt{N}$	−0.155	0.021
SPR	$\beta_1^{(1)} \sim$	Intercept	−3.624	3.407
SPR		ln(Dg)	13.373	0.978
SPR	$\beta_2^{(1)} \sim$	Intercept	39.737	2.339
SPR		ln(*N*)	−3.074	0.352
SPR		$\sqrt{\frac{G_{\text{species}}}{G}}$	−3.320	0.732
FIR	$\beta_1^{(1)} \sim$	Intercept	−11.148	4.674
FIR		ln(Dg)	15.391	1.329
FIR	$\beta_2^{(1)} \sim$	Intercept	−8.309	4.210
FIR		$\ln(G_{\text{species}})$	−0.713	0.177
FIR		ln(Ddom)	7.559	1.109
SYM	$\beta_1^{(1)} \sim$	Intercept	−18.813	4.635
SYM		ln(Dg)	13.989	1.395
SYM		$\sqrt{\frac{G_{\text{species}}}{G}}$	3.879	1.373
SYM	$\beta_2^{(1)} \sim$	Intercept	8.318	1.596
SYM		$\sqrt{N}$	−0.135	0.030
SYM		Ddom	0.106	0.025
EH	$\beta_1^{(1)} \sim$	Intercept	7.434	7.004
EH		ln(Dg)	6.159	2.201
EH		$\ln\left(\frac{G_{\text{species}}}{G}\right)$	1.473	0.360
EH	$\beta_2^{(1)} \sim$	Intercept	15.069	6.900
EH		ln(Dg)	−0.670	1.810
EH		$\sqrt{N}$	−0.185	0.054

3.4. Response curves

All *H* and CL models except the CL model for FIR species include Dg as a fixed-effect. Applying a logarithmic transformation to Dg in most cases resulted in better performance than using raw values. Both *H* and the CL increase with an increase in Dg (Fig. 2). For BE, minimal DBH values (less than 9 cm) and high Dg result in a slightly smaller *H* than a lower Dg. This behaviour is explained by the complex stand structures typical of many Romanian forests. In stands with large Dg, trees in smaller diameter classes often grow beneath the canopy, which slows down or even stops their *H* growth. Conversely, with smaller Dg, the stand structure tends to be more homogeneous, allowing for more rapid *H* growth due to increased competition for light.

A similar pattern is observed with Ddom (Supplementary Material Fig. B1). When the difference between Dg and Ddom is large, the *H* is lower compared to when this difference is smaller, for the same DBH

Table 4
Fixed parameters corresponding to the CL model for the main five species in the study area.

Species	Fixed Param.	Term	Estimate	Std. Error
BE	$\beta_3^{(2)} \sim$	Intercept	0.789×10^{-1}	0.369
BE		ln(Dg)	0.672	0.117
BE		Gini	−1.081	0.352
BE	$\beta_4^{(2)} \sim$	Intercept	-0.498	0.794×10^{-1}
BE		ln(Dg)	-0.324	0.234×10^{-1}
BE		$G_{species}$	0.124×10^{-2}	0.376×10^{-3}
BE		BALMOD	0.150×10^{-1}	0.134×10^{-2}
SPR	$\beta_3^{(2)} \sim$	Intercept	4.856	0.484
SPR		ln(Dg)	−0.392	0.151
SPR		$\ln(G_{species})$	0.219×10^{-1}	0.402×10^{-1}
SPR		Gini	−1.516	0.604
SPR	$\beta_4^{(2)} \sim$	Intercept	−1.851	0.047
SPR		BALMOD	0.957×10^{-2}	0.167×10^{-2}
SPR		$\sqrt{G}$	0.197×10^{-1}	0.649×10^{-2}
FIR	$\beta_3^{(2)} \sim$	$\beta_3^{(2)}$	3.403	0.113
FIR	$\beta_4^{(2)} \sim$	Intercept	−1.656	0.045
FIR		$\sqrt{\text{BALMOD}}$	0.177×10^{-1}	0.790×10^{-2}
FIR		$\ln(G_{species})$	0.220×10^{-1}	0.930×10^{-2}
FIR		Gini	−0.313	0.110
SYM	$\beta_3^{(2)} \sim$	Intercept	0.688	0.479
SYM		BAL	0.148×10^{-1}	0.539×10^{-2}
SYM		Ddom	0.666×10^{-2}	0.904×10^{-2}
SYM		$\sqrt{N}$	0.153×10^{-1}	0.106×10^{-1}
SYM	$\beta_4^{(2)} \sim$	Intercept	−1.177	0.060
SYM		Dg	-0.750×10^{-2}	0.164×10^{-2}
EH	$\beta_3^{(2)} \sim$	Intercept	3.908	0.635
EH		ln(Dg)	−0.821	0.226
EH		$\sqrt{\text{BALMOD}}$	0.918×10^{-1}	0.110
EH	$\beta_4^{(2)} \sim$	Intercept	−1.522	0.037
EH		$\ln\left(\frac{G_{species}}{G}\right)$	-0.588×10^{-1}	0.122×10^{-1}

value. Height increases with higher values of N (Supplementary Material Fig. B2), which is consistent with the trees known biological behaviour. In crowded stands, trees prioritize biomass allocation to H growth over diameter growth, thereby enhancing their competitive ability to win a better position in the canopy. Similar to H, CL increases with an increase in Dg however the increase in SPR is limited while for BE and SYM the CL variation explained by Dg is high (Supplementary Material Fig. B3).

Species mixture was modelled by incorporating $G_{species}$ into the model. Various formulations, including logarithmic and square root transformations, performed better than using raw values. In all cases, H of the species increased with an increase in $G_{species}$ (Fig. 2).

In contrast, the CL model exhibits an opposite pattern. For the BE, SPR, and FIR species, CL values decrease as $G_{species}$ increases, whereas they increase for EH (Supplementary Material Fig. B4). The tree-level competition was modelled using the BALMOD variable (Fig. 3). In our dataset, BALMOD values range from 0 to 10, where 0 represents no competition and 10 indicates very high competition experienced by the tree. As BALMOD increases, CL decreases. A similar trend is observed with the BAL variable, where for the EH species, CL decreases as BAL increases (Supplementary Material Fig. B5).

The Gini index was found to explain the variability CL for BE, SPR, and FIR species (Fig. 3). As structural diversity, measured by the variation in DBH and represented by the Gini index, increases, so does CL.

3.5. Multivariate model calibration

3.5.1. When measurements from both response variables are available

Fifty CUs with either one or two SP were used to test the three sampling strategies for BE and SPR, while twenty CUs were used for each of the other three species. The three sampling strategies employed yielded similar results, with only marginal differences among them (Fig. 4). No single strategy consistently outperformed the others, as each demonstrated varying effectiveness depending on the model and species. Notably, a calibration strategy that performed well for the H model did not necessarily do so for the CL model. However, when evaluating how often each calibration strategy outperformed the others across different species and number of trees used in the calibration, a few patterns emerged. For the BE species, the mean tree sampling strategy consistently performed better for both the H and CL models. A similar trend was observed for the FIR species when calibrating the H model. In contrast, for the SPR species, sampling from the extremes was the best calibration strategy for the H model, while random selection proved most effective for the CL model. For the other species, no clear preference for any calibration strategy was evident, as each performed equally well. Overall,

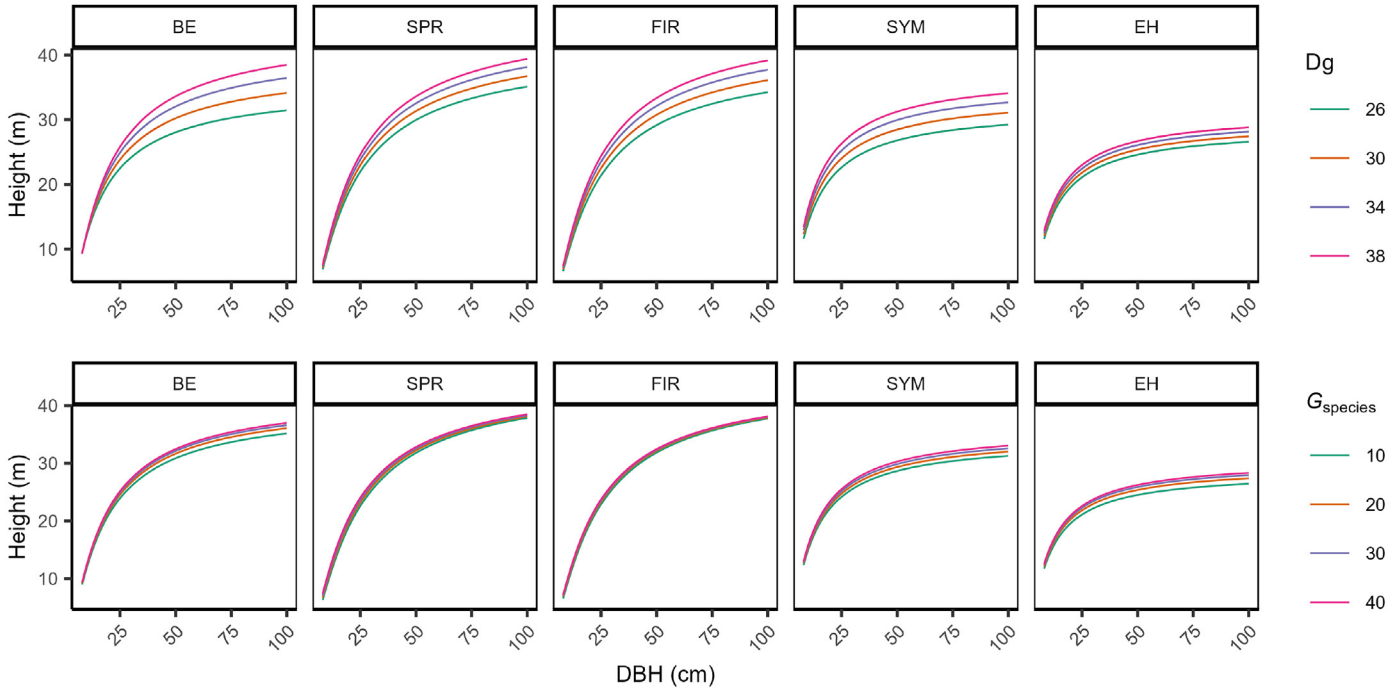

Fig. 2. Tree height response to changes in Dg and the $G_{species}$ stand variables, with all other variables held constant.

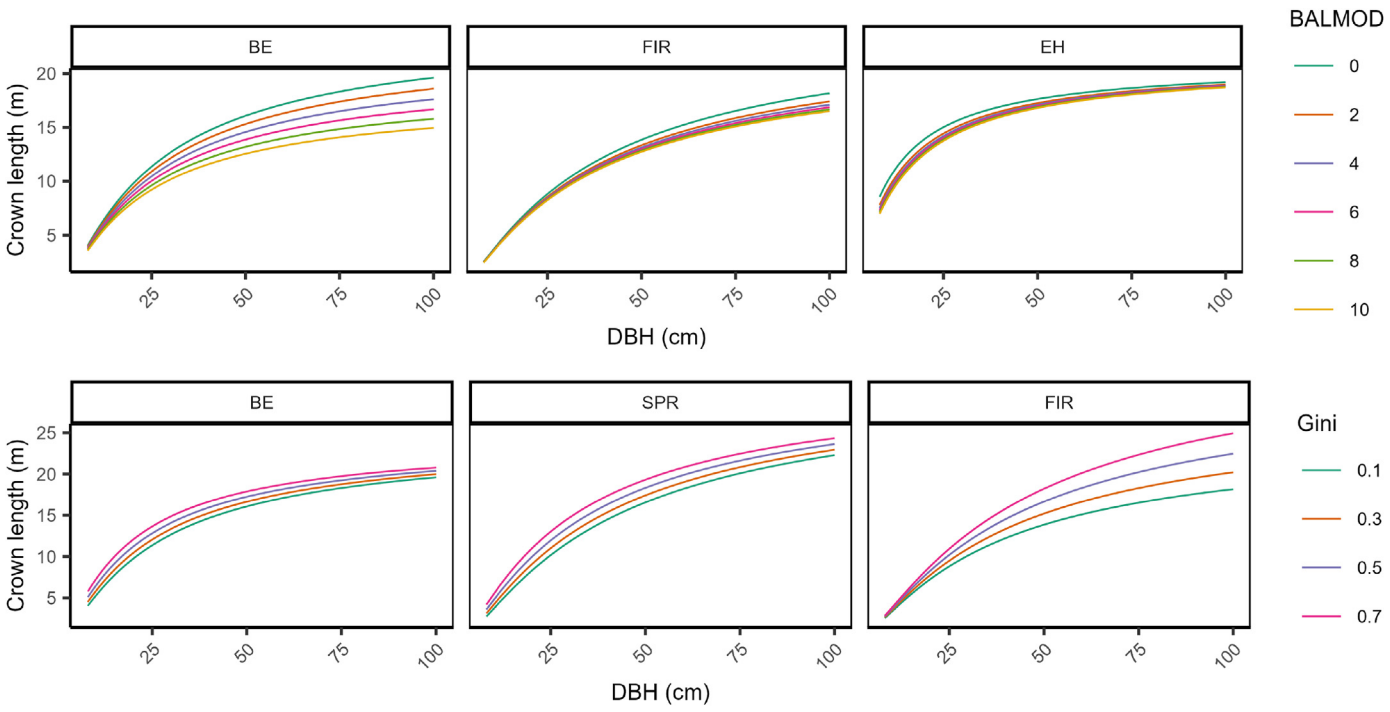

Fig. 3. Crown length response to changes in BALMOD and the Gini index, with all other variables held constant.

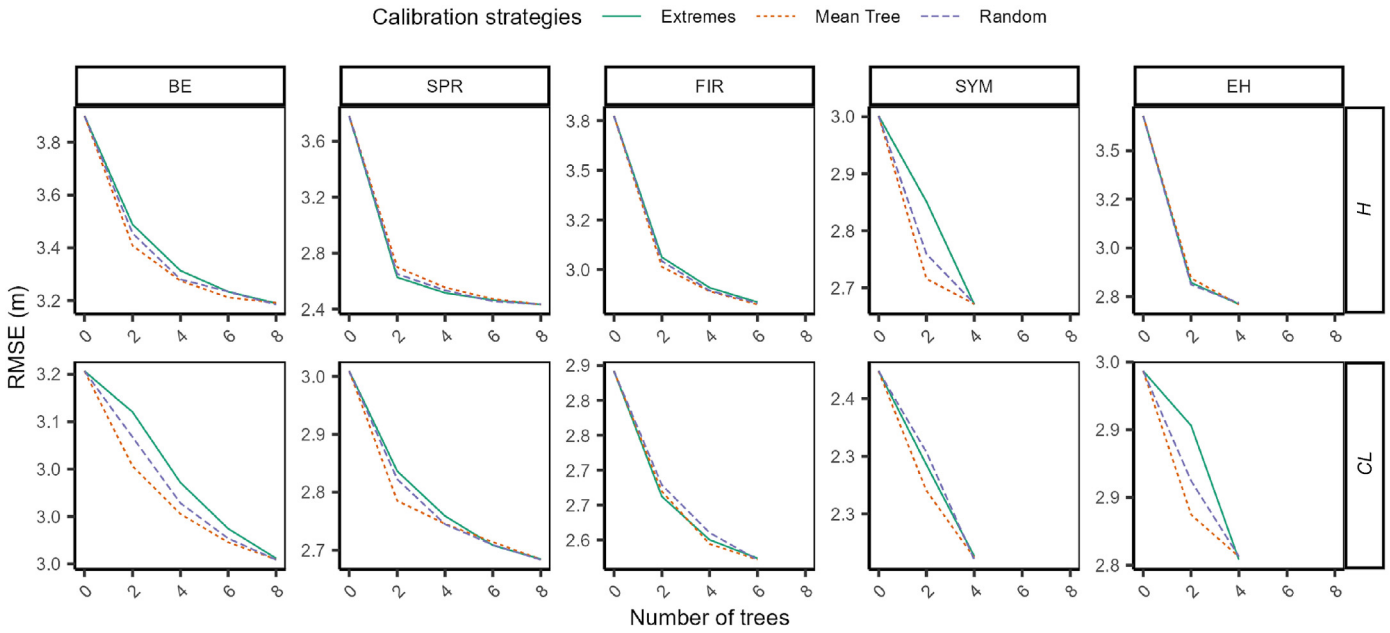

Fig. 4. Multivariate model performance calibrated assessed under three different calibration strategies, with varying number of trees. In this process, both *H* and CL measurements were used to predict the random-effects for the *H* and CL models.

it is clear that employing a calibration strategy generally increases model accuracy more effectively than relying on a random selection of trees.

3.5.2. *When only H measurements are available*

In comparison to the scenario where observations for both response variables are available, cross-model calibration yields only a marginal improvement in the RMSE statistic for the CL model (Fig. 5). Although the reduction in RMSE with cross-model calibration is substantially less than that achieved when two CL observations were used for calibration, there are still improvements in model performance. This suggests that cross-model calibration can potentially improve the accuracy of CL predictions relative to fixed-effects prediction and could serve as a valuable alternative for refining CL estimates in the absence of direct CL observations. Consistent with the first scenario, no definitive pattern emerges among the three calibration strategies.

4. Discussion and conclusions

4.1. *Simple model selection*

Tree growth is typically modelled using explanatory variables that fall into three main categories: tree size, competition, and site characteristics

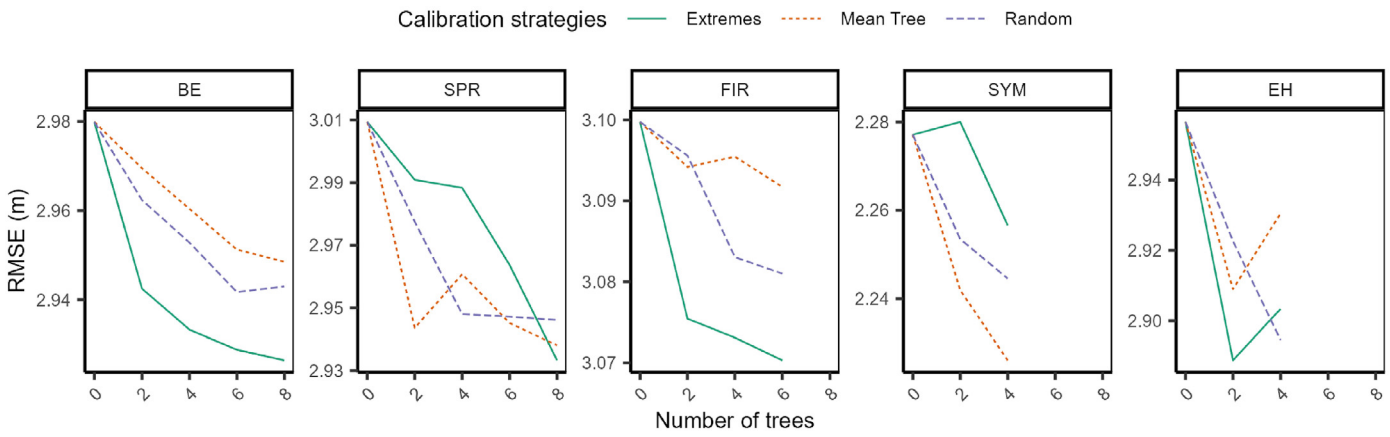

Fig. 5. Crown length model performance cross-calibrated assessed under three different calibration strategies, with varying number of trees. In the calibration process, only *H* measurements were used to predict the random-effects for the *H* and CL models.

(Weiskittel et al., 2011). Both CL and *H* can be incorporated into these models as part of the first two components, as they reflect the tree's current size and its history of competition.

Therefore, accurate estimates of tree growth are closely tied to the behaviour of *H* and CL models. Consistency and logical behaviour in these models are essential for making reliable predictions.

Our study found that similar allometric formulations performed well across multiple species, despite observing distinct allometric relationships for *H* and CL. This is unusual, as most studies report different allometric formulations for each species or dataset (Temesgen et al., 2014; Mehtätalo et al., 2015). Many studies, though, fail to adopt a holistic approach to comparing model performance, often focusing solely on RMSE improvements. Our study, in contrast, assessed both ME and RMSE for fixed and random-effects predictions. However, it is not uncommon to apply a single model formulation across all species, prioritizing the ease of parameter estimation, computation time, and transferability over accuracy (Sharma and Parton, 2007).

We found that the Curtis model (Curtis, 1967) outperformed the other two-parameter models tested for *H*. While Mehtätalo et al. (2015) noted that no single model consistently performs best in all situations, they observed that both the Näslund (1936) and Curtis (1967) models provided satisfactory fits across various datasets. In contrast, Ciceu et al. (2020) reported that the Wykoff model (Wykoff et al., 1982) performed better for SPR in Romanian forests. However, their findings were based on unmanaged, uneven-aged stands with a smaller sample size, which may explain the differences in results.

For the CL model, we applied an exponential transformation to the *b* parameter (see Eq. 3) (Mehtatalo and Kansanen, 2022), which outperformed the classic formulation by Näslund (1936) (results not shown). Similarly, Lee et al. (2021) applied an exponential transformation to both parameters to ensure positive values and logical behaviour in their model.

We focused exclusively on two-parameter models, as our goal was to extend these models by incorporating additional variables. Although three-parameter models have been shown to perform better in some cases (Huang et al., 1992), the difference in accuracy is relatively small. Two-parameter models offer the advantage of achieving similar accuracy with fewer parameters, resulting in a more parsimonious model.

4.2. Multivariate approach

We selected a mixed-effects approach to models *H* and CL due to the hierarchical nature of our sampling design. Mixed-effects models are the most frequent approach for modelling the *H*-DBH relationship (Ciceu et al., 2023). While various algorithms (Skudnik and Jevšenak, 2022; Yu et al., 2024) have demonstrated comparable overall accuracy, we favoured mixed-effects models for their ability to manage hierarchical data structures and their straightforward calibration. Although *H* and CL are commonly modelled using univariate models (Mehtätalo, 2005; Saud et al., 2016; Bronisz and Mehtätalo, 2020a; Han et al., 2021; Li et al., 2020), we emphasized on their inherent interrelation. Our multivariate approach accounted for the residual correlation between *H* and CL, revealing a strong correlation of residuals (ranging from 0.462 to 0.677), which validated our decision to model these variables jointly. This positive residual correlation indicates that larger tree *H* are associated with greater CL. For comparison, Bronisz and Mehtätalo (2020b) reported a weaker residual correlation when jointly modelling tree *H* and biomass components, with the highest correlation observed for stem biomass component ($r = 0.256$). In contrast, Lappi (1991) found a stronger correlation between tree *H* and volume ($r = 0.795$). Their research demonstrates that higher *H* correlates with greater biomass and volume.

In line with our research topic, Zhou et al. (2022) used a model system to estimate *H*, CL, and HCB simultaneously through nonlinear seemingly unrelated regression, though without considering the hierarchical data structure. They ensured additive compatibility of CL and HCB with *H* by fitting all three models simultaneously. Eerikäinen (2009) on the other hand, incorporated data structure in their multivariate seemingly unrelated mixed-effects model for predicting *H* and CR, but opted for a linear model. In contrast with these two studies, we chose a nonlinear mixed-effects approach that incorporated the complex hierarchical structure of our data, enabling us to estimate cross-model random-effect correlations.

We observed a strong cross-model random-effects correlation across all species. This result is consistent with Bronisz and Mehtätalo (2020b), who reported robust cross-model random-effects correlation, with coefficients reaching up to 0.952 for certain biomass components. Similarly, Lappi (1991) found high correlations between the random-effects of volume and *H* models, with a maximum coefficient of $r = 0.982$. In contrast, Eerikäinen (2009) reported the highest correlation of $r = -0.826$ between the random-effects of *H* and CR models. These strong correlations facilitate cross-model calibration, reducing sampling effort and enhancing model performance.

The observed residual error and random-effects correlation align with expectations, as tree-size variables are biologically constrained to maintain specific proportions for structural stability. These constraints ensure proportional growth rates across different tree components, resulting in strong allometric relationships that can be leveraged in model development.

Additionally, modelling *H* and CL jointly addresses a common issue in studies predicting crown characteristics, where *H* is often used as a predictor (Sattler and LeMay 2011; Rijal et al., 2012). By fitting both variables simultaneously through a multivariate approach, we preserve

the logical relationship between *H* and CL, leading to consistent and realistic CL estimates that remain lower than *H* for the same tree. This joint modelling improves the accuracy of fixed-effect parameter estimates and provides a more realistic prediction of both variables, reinforcing the importance of considering such strong correlations in growth models.

4.3. Model behaviour

The study area is characterized by multi-species stands with a complex structure, resulting from close-to-nature forest management practices in Romania. This aspect influenced many of our decisions regarding the variables tested to model the variation in *H* and CL. We used only stand-level predictors in the *H* model, which can be estimated using angle-count sampling without a full stand inventory. This makes the *H* model applicable in forest management applications, such as stand volume and biomass estimation. The most important variable for explaining *H* variability was Dg, which is closely related to stand development. Height and CL increase with an increase in Dg, reflecting a logical ageing pattern. We avoided using dominant height as an additional predictor because it is typically estimated based on stand age, which can be challenging to determine in naturally regenerated stands with long regeneration periods. Also, measuring dominant height by assessing the 100 thickest trees per hectare would require a large number of *H* measurements. Instead, we found that calibrating the model with fewer *H* measurements but using a targeted sampling strategy, is a more efficient method for obtaining accurate *H* estimates.

We observed that the increase in *H* estimates in response to interspecific competition varied among species. Although a general trend emerged where pure stands yielded higher *H* values compared to mixed stands, the degree of *H* increase differed among species. For example, BE exhibited clear increases in *H*, whereas SPR showed more modest gains, yet all species demonstrated an overall increase. This variation in response aligns with the findings of Forrester et al. (2017), who reported smaller tree *H* in more diverse forests across multiple European ecosystems. In pure stands, trees of the same species generally exhibit similar *H* growth patterns, leading to increased competition for light. In mixed stands, however, species allocate biomass to *H* growth at different stages of development and in varying amounts, resulting in asynchronous *H* increments. This asynchrony can benefit certain species, allowing them to reach the top canopy more easily and then slow their *H* growth once they achieve dominance. A similar pattern was observed with the Ddom variable, where a wider diameter distribution correlated with lower *H* estimates. This likely reflects the increased stand complexity typical of uneven-aged or multilayered forests, where a few dominant trees secure their place in the canopy and subsequently reduce their *H* growth earlier compared with those in even-aged stands. Similarly, the *H* model reports higher estimates for stands with a greater number of trees compared to those with fewer trees. This is expected, as denser stands exhibit competition-driven acceleration in *H* increment.

The CL model displayed an opposite response to interspecific competition compared to the *H* model. Except for EH, CL estimates for a species increased as its share of basal area in the stand decreased. These findings align with those reported by Hilmers et al. (2024), who observed longer CL when BE immediate neighbours were Scots pine rather than other BE trees. They attributed this to differing light requirements and *H* increment strategies among species. Another factor could be the more efficient use of vertical space. The CL model produced higher CL estimates in stands with increased structural complexity compared to homogeneous stands. Although the Gini coefficient was calculated for DBH, the variation in DBH also indicates variation in vertical structure, leading to light being intercepted by a larger portion of the tree stem across multiple species. The competition effect on CL was modelled using BALMOD, which proved superior to both BAL and RD as competition indices. Similar results were found by Kahriman et al. (2018), who reported that BALMOD outperformed 18 other distance-dependent and distance-independent competition indices (including the ones tested here) in predicting the diameter increment of Calabrian pine. The strength of BALMOD lies in its formulation, which integrates aspects of both BAL and RS, making it particularly effective for our study, which involved data from a wide range of stand densities. Although we modified the original BALMOD formulation by Schröder and Gadow (1999) by substituting dominant height with Dg for easier calculation, the model's behaviour remained nearly equivalent due to the strong correlation between Dg and dominant height.

4.4. Model calibration

Utilizing a mixed-effects modelling approach enables users to calibrate the model by predicting random-effects for a new plot. Various studies (Bronisz and Mehtätalo, 2020a; Patrício et al., 2022; Ciceu et al., 2022; Siipilehto et al., 2023) have examined different sampling strategies for random-effects calibration, which can generally be categorized into two main types: size-driven calibrations, focusing on specific tree sizes, such as those near the minimum, mean, or maximum DBH/*H*; and probability-driven calibrations, which employ percentiles or quantiles, or attempt to mirror the distribution of tree sizes within the sample (Ciceu et al., 2023). There is ongoing debate regarding the most effective sampling strategy, with studies reporting mixed results (Dorado et al., 2006; Gómez-García et al., 2014; Hofiço et al., 2020; Ogana et al., 2020), primarily due to the differences in the functions used for model fitting, as well as variations in the data and variables involved. We examined two common scenarios in forestry practice concerning the availability of new observations for two response variables. Our results demonstrate that when observations for both response variables are available, calibrating the model - even with a limited number of observations - substantially outperforms predictions based solely on fixed-effects. Furthermore, when planning sampling efforts for calibration, strategies that involve sampling trees close to the mean DBH or from the extremes of the DBH distribution yield better results compared to random sampling.

In the second scenario, where only *H* measurements are available, using cross-model random-effects predictions led to a marginal improvement in CL estimates compared to predictions based solely on the fixed-effects component. This modest enhancement is due to the reduced variability explained by the random-effects in the CL model. This can be also observed when calibrating the model with observations from both response variables. While the fixed-effects account for a substantial portion of the variation in CL, the random-effects contribute less to the improvement in CL estimates compared to their impact on *H*. However, this still leads to a 2% increase in accuracy for BE compared with the fixed-effects prediction. Greater improvements could have been realized if we had focused on modelling HCB alongside *H*. Our preliminary work (results not shown) indicated that while fixed-effects alone resulted in a poor model fit for HCB compared to the CL model, the random-effects explained a larger portion of the variation. This approach led to an increase in accuracy of approximately 12% by employing the cross-model random-effects predictions. As we aimed for a maximal accuracy of the model based on the fixed-effects we opted for predicting CL alongside *H*.

4.5. Potential future applications of NSURME in individual tree growth modelling

Many DBH increment models developed based on the mixed-effects modelling framework are challenging to calibrate due to the frequent lack of direct DBH increment in new plots. While DBH increment data is available in permanent plots - such as those used in monitoring networks and national forest inventories - it is often missing in standard forest management scenarios, where growth models project stand development. Additionally, obtaining DBH increment measurements through increment cores is impractical for large-scale applications.

To overcome this limitation, a promising approach is to jointly model DBH increment, *H*, and CL. This multivariate approach enhances model

coherence and realism, leading to more accurate DBH increment estimates. Moreover, it enables the cross-calibration of the DBH increment model in new stands using easily measurable variables like *H* and CL, making the model more flexible.

Adopting this approach makes it possible to develop a fully calibrated individual-tree growth model, resulting in stand-specific predictions and improved decision-making in forest management.

CRediT authorship contribution statement

Albert Ciceu: Writing – original draft, Visualization, Software, Methodology, Investigation, Formal analysis, Data curation, Conceptualization. **Ştefan Leca:** Writing – review & editing, Resources, Project administration, Methodology, Investigation, Funding acquisition. **Ovidiu Badea:** Writing – review & editing, Resources, Project administration, Methodology, Funding acquisition. **Lauri Mehtätalo:** Writing – review & editing, Supervision, Methodology.

Declaration of competing interest

The authors declare that they have no known competing financial interests or personal relationships that could have appeared to influence the work reported in this paper.

Acknowledgements

This work was supported by the European Union and the Romanian Government through the Competitiveness Operational Programme 2014–2020, under the project "Increasing the economic competitiveness of the forestry sector and the quality of life through knowledge transfer, technology and CDI skills" (CRESFORLIFE), ID P 40 380/105506, subsidiary contract no. 17/2020 and partially by the FORCLIMSOC Nucleu Programme (Contract 12N/2023), project PN 23090101 and CresPerfInst project (Contract 34PFE/December 30, 2021) "Increasing the institutional capacity and performance of INCDS 'Marin Drăcea' in RDI activities - CresPerfInst". LM was financially supported by the Research Council of Finland's flagship ecosystem for Forest-Human-Machine Interplay – Building Resilience, Redefining Value Networks and Enabling Meaningful Experiences (UNITE) (decision number 357909).

Supplementary data

Supplementary data to this article can be found online at https://doi.org/10.1016/j.fecs.2025.100322.

References

Badea, O., 2008. Manual on Methodology for Long Term Monitoring of Forest Ecosystems Status under Air Pollution and Climate Change Influences. Ed. Silvica, Bucharest, Romania, pp. 1–100 (in Romanian).
Badea, O., Patrascoiu, N., 1999. The national forest survey network (2 × 2 and 2 × 4 km). Forest Cond. Monitor. Romania 1990–1996, 7–14.
Bronisz, K., Mehtätalo, L., 2020a. Mixed-effects generalized height–diameter model for young silver birch stands on post-agricultural lands. For. Ecol. Manag. 460, 117901.
Bronisz, K., Mehtätalo, L., 2020b. Seemingly unrelated mixed-effects biomass models for young silver birch stands on post-agricultural lands. Forests 11 (4), 381.
Burkhart, H.E., Tomé, M., 2012. Modeling Forest Trees and Stands. Springer, Dordrecht.
Calama, R., Montero, G., 2004. Interregional nonlinear height diameter model with random coefficients for stone pine in Spain. Can. J. For. Res. 34 (1), 150–163.
Ciceu, A., Bronisz, K., Garcia-Duro, J., Badea, O., 2022. Age-independent diameter increment models for mixed mountain forests. Eur. J. For. Res. 141 (5), 781–800.
Ciceu, A., Chakraborty, D., Ledermann, T., 2023. Examining the transferability of height–diameter model calibration strategies across studies. Forestry, cpad063.
Ciceu, A., Garcia-Duro, J., Seceleanu, I., Badea, O., 2020. A generalized nonlinear mixed-effects height–diameter model for Norway spruce in mixed-uneven aged stands. For. Ecol. Manag. 477, 118507.
Ciceu, A., Pitar, D., Badea, O., 2021. Modeling the diameter distribution of mixed uneven-aged stands in the south western carpathians in Romania. Forests 12 (7), 958.
Cochran, W.G., 1963. Sampling Techniques, second ed. John Wiley & Sons, New York.
Curtis, R.O., 1967. Height-diameter and height-diameter-age equations for second-growth douglas-fir. For. Sci. 13 (4), 365–375.
Dorado, F.C., Diéguez-Aranda, U., Anta, M.B., Rodríguez, M.S., von Gadow, K., 2006. A generalized height–diameter model including random components for radiata pine plantations in northwestern Spain. For. Ecol. Manag. 229 (1–3), 202–213.
Eerikäinen, K., 2009. A multivariate linear mixed-effects model for the generalization of sample tree heights and crown ratios in the Finnish national forest inventory. For. Sci. 55 (6), 480–493.
Forrester, D.I., Benneter, A., Bouriaud, O., Bauhus, J., 2017. Diversity and competition influence tree allometric relationships–developing functions for mixed-species forests. J. Ecol. 105 (3), 761–774.
Giurgiu, V., 1968. Cercetări privind inventarierea statistică a arboretelor. Centrul de Documentare Tehnică pentru Economia Forestieră.
Gómez-García, E., Diéguez-Aranda, U., Castedo-Dorado, F., Crecente-Campo, F., 2014. A comparison of model forms for the development of height-diameter relationships in even-aged stands. For. Sci. 60 (3), 560–568.
Hall, D.B., Clutter, M., 2004. Multivariate multilevel nonlinear mixed effects models for timber yield predictions. Biometrics 60 (1), 16–24.
Han, Y., Lei, Z., Ciceu, A., Zhou, Y., Zhou, F., Yu, D., 2021. Determining an accurate and cost-effective individual height-diameter model for Mongolian pine on sandy land. Forests 12 (9), 1144.
Hann, D.W., Bluhm, A., Hibbs, D., 2011. Development and evaluation of the tree-level equations and their combined stand-level behavior in the red alder plantation version of organon. Forest Biometrics Research Note 1. https://archive-cips.forestry.oregonstate.edu/sites/cips/files/Development and Evaluation of RAP-ORGANON %281%29.pdf. (Accessed 15 January 2025).
Hasenauer, H., Monserud, R.A., Gregoire, T.G., 1998. Using simultaneous regression techniques with individual-tree growth models. For. Sci. 44 (1), 87–95.
Hilmers, T., Mehtätalo, L., Bielak, K., Brazaitis, G., del Río, M., Ruiz-Peinado, R., Schmied, G., Uhl, E., Pretzsch, H., 2024. Towards resource-efficient forests: mixing species changes crown biomass allocation and improves growth efficiency. Plants People Planet 7, 117–132.
Hofiço, N.S.A., Costa, E.A., Fleig, F.D., Finger, C.A.G., Hess, A.F., 2020. Height-diameter relationships for *Eucalyptus grandis* Hill Ex. maiden in Mozambique: using mixed-effects modeling approach. Cerne 26 (2), 183–192.
Huang, S., Titus, S.J., Wiens, D.P., 1992. Comparison of nonlinear height–diameter functions for major alberta tree species. Can. J. For. Res. 22 (9), 1297–1304.
Kahriman, A., Şahin, A., Sönmez, T., Yavuz, M., 2018. A novel approach to selecting a competition index: the effect of competition on individual-tree diameter growth of calabrian pine. Can. J. For. Res. 48 (10), 1217–1226.
Lappi, J., 1991. Calibration of height and volume equations with random parameters. For. Sci. 37 (3), 781–801.
Leca, S., Popa, I., Chivulescu, S., Popa, A., Pitar, D., Dobre, A.-C., Pascu, I.-S., Apostol, B., Badea, O., 2023. Structure and diversity in a periurban forest of bucharest, Romania. Ann. For. Res. 66 (1), 139–153.
Lee, D., Siipilehto, J., Hynynen, J., 2021. Models for diameter distribution and tree height in hybrid aspen plantations in southern Finland. Silva Fenn. 55, 10612.
Li, Y., Wang, W., Zeng, W., Wang, J., Meng, J., 2020. Development of crown ratio and height to crown base models for masson pine in southern China. Forests 11 (11), 1216.
Lintunen, A., Kaitaniemi, P., 2010. Responses of crown architecture in *Betula pendula* to competition are dependent on the species of neighbouring trees. Trees 24, 411–424.
Mäkelä, A., Valentine, H.T., 2006. Crown ratio influences allometric scaling in trees. Ecology 87 (12), 2967–2972.
Mehtätalo, L., 2005. Height-diameter models for Scots pine and birch in Finland. Silva Fenn. 39, 55–66.
Mehtätalo, L., de Miguel, S., Gregoire, T.G., 2015. Modeling height-diameter curves for prediction. Can. J. For. Res. 45 (7), 826–837.
Mehtatalo, L., Kansanen, K., 2022. Lmfor: functions for forest biometrics. R package version 1.6. https://CRAN.R-project.org/package=lmfor (Accessed 15 January 2025).
Mehtatalo, L., Lappi, J., 2020. Biometry for Forestry and Environmental Data: with Examples in R. Chapman and Hall/CRC, New York.
Monserud, R.A., Sterba, H., 1999. Modeling individual tree mortality for Austrian forest species. For. Ecol. Manag. 113 (2–3), 109–123.
Näslund, M., 1936. Skogsförsöksanstaltens gallringsförsök i tallskog. Meddelanden Från Statens Skogsförsöksanstalt. https://pub.epsilon.slu.se/10159/1/medd_statens_skogsforskningsanst_029_01.pdf (Accessed 15 January 2025).
Ogana, F.N., Corral-Rivas, S., Gorgoso-Varela, J.J., 2020. Nonlinear mixed-effect height-diameter model for *Pinus pinaster* Ait. and *Pinus radiata* D. Don. Cerne 26, 150–161.
Oliveira, I.R., Bouillet, J.-P., Guillemot, J., Brandani, C., Bordron, B., Frayret, C., Laclau, J.-P., Ferraz, A., Gonçalves, J.L.M., Le Maire, G., 2024. Changes in light use efficiency explains why diversity effect on biomass production is lower at high planting density in mixed-species plantations of *Eucalyptus grandis* and *Acacia mangium*. For. Ecol. Manag. 554, 121663.
Patrício, M.S., Dias, C.R., Nunes, L., 2022. Mixed-effects generalized height-diameter model: a tool for forestry management of young sweet chestnut stands. For. Ecol. Manag. 514, 120209.
Pinheiro, J., Bates, D., 2000. Mixed-effects Models in S and S-PLUS. Springer, New York.
Pretzsch, H., 2021. Tree growth as affected by stem and crown structure. Trees (Berl.) 35 (3), 947–960.
Pretzsch, H., Biber, P., Ďurskỳ, J., 2002. The single tree-based stand simulator silva: construction, application and evaluation. For. Ecol. Manag. 162 (1), 3–21.
R Core Team, 2022. Nlme: linear and nonlinear mixed effects models. R package version 3, 1–157. https://CRAN.R-project.org/package=nlme.
Rijal, B., Weiskittel, A.R., Kershaw Jr, J.A., 2012. Development of height to crown base models for thirteen tree species of the North American Acadian region. For. Chron. 88 (1), 60–73.

Sattler, D.F., LeMay, V., 2011. A system of nonlinear simultaneous equations for crown length and crown radius for the forest dynamics model SORTIE-ND. Can. J. For. Res. 41 (8), 1567–1576.
Saud, P., Lynch, T.B., Anup, K.C., Guldin, J.M., 2016. Using quadratic mean diameter and relative spacing index to enhance height–diameter and crown ratio models fitted to longitudinal data. Forestry 89 (2), 215–229.
Schröder, J., Gadow, K.v., 1999. Testing a new competition index for maritime pine in northwestern Spain. Can. J. For. Res. 29 (2), 280–283.
Schumacher, F.X., 1939. A new growth curve and its application to timber-yield studies. J. For. 37, 819–820.
Sharma, M., Parton, J., 2007. Height–diameter equations for boreal tree species in ontario using a mixed-effects modeling approach. For. Ecol. Manag. 249 (3), 187–198.
Siipilehto, J., Sarkkola, S., Nuutinen, Y., Mehtätalo, L., 2023. Predicting height-diameter relationship in uneven-aged stands in Finland. For. Ecol. Manag. 549, 121486.
Skudnik, M., Jevšenak, J., 2022. Artificial neural networks as an alternative method to nonlinear mixed-effects models for tree height predictions. For. Ecol. Manag. 507, 120017.
Stenberg, P., Kuuluvainen, T., Kellomäki, S., Grace, J.C., Jokela, E.J., Gholz, H.L., 1994. Crown structure, light interception and productivity of pine trees and stands. Ecol. Bull. 43, 20–34.
Temesgen, H., Zhang, C., Zhao, X., 2014. Modelling tree height–diameter relationships in multi-species and multi-layered forests: a large observational study from northeast China. For. Ecol. Manag. 316, 78–89.
Thurnher, C., Klopf, M., Hasenauer, H., 2017. Moses–a tree growth simulator for modelling stand response in central Europe. Ecol. Model. 352, 58–76.
Tomppo, E., Gschwantner, T., Lawrence, M., McRoberts, R.E., 2010. National Forest Inventories. Pathways for Common Reporting. Springer, Dordrecht. pp. 541–553.
Trincado, G., VanderSchaaf, C.L., Burkhart, H.E., 2007. Regional mixed-effects height–diameter models for loblolly pine (*Pinus taeda* L.) plantations. Eur. J. For. Res. 126, 253–262.
Weiskittel, A.R., Hann, D.W., Kershaw Jr, J.A., Vanclay, J.K., 2011. Forest Growth and Yield Modeling. John Wiley & Sons.
Wykoff, W., Crookston, N.L., Stage, A.R., 1982. User's Guide to the Stand Prognosis Model, Vol. 133. US Department of Agriculture, Forest Service, Intermountain Forest and Range Experiment Station.
Yang, S.-I., Brandeis, T.J., Helmer, E.H., Oatham, M.P., Heartsill-Scalley, T., Marcano-Vega, H., 2022. Characterizing height-diameter relationships for caribbean trees using mixed-effects random forest algorithm. For. Ecol. Manag. 524, 120507.
Yu, Y., Zhou, Z., Sharma, R.P., Zhang, L., Du, M., Zhang, H., 2024. Comparing crown ratio models for spruce-fir broadleaved mixed forests using beta regression and random forest algorithm. Comput. Electron. Agric. 225, 109302.
Zellner, A., 1962. An efficient method of estimating seemingly unrelated regressions and tests for aggregation bias. J. Am. Stat. Assoc. 57 (298), 348–368.
Zhou, Z., Fu, L., Zhou, C., Sharma, R.P., Zhang, H., 2022. Simultaneous compatible system of models of height, crown length, and height to crown base for natural secondary forests of Northeast China. Forests 13 (2), 148.
Zhu, Z., Kleinn, C., Nölke, N., 2021. Assessing tree crown volume-a review. Forestry 94 (1), 18–35.